Journal of Ceramic Processing Research. Vol. 19, No. 5, pp. 401~406 (2018)

J O U R N A L O F
Ceramic Processing Research

Density control of ZnO nanorod arrays using ultrathin seed layer by atomic layer deposition

Seokyoon Shin[a,1], Joohyun Park[b,1], Juhyun Lee[a], Hyeongsu Choi[a], Hyunwoo Park[a], Minwook Bang[a] Kyungpil Lim[a], Hyunjun Kim[a] and Hyeongtag Jeon[a,b]

[a]*Division of Materials Science and Engineering, Hanyang University, Seoul, 04763, Korea*
[b]*Division of Nano-scale Semiconductor Engineering, Hanyang University, Seoul 04763, Korea*

We investigated the effect of ZnO seed layer thickness on the density of ZnO nanorod arrays. ZnO has been deposited using two distinct processes consisting of the seed layer deposition using ALD and subsequent hydrothermal ZnO growth. Due to the coexistence of the growth and dissociation during ZnO hydrothermal growth process on the seed layer, the thickness of seed layer plays a critical role in determining the nanorod growth and morphology. The optimized thickness resulted in the regular ZnO nanorod growth. Moreover, the introduction of ALD to form the seed layer facilitates the growth of the nanorods on ultrathin seed layer and enables the densification of nanorods with a narrow change in the seed layer thickness. This study demonstrates that ALD technique can produce densely packed, virtually defect-free, and highly uniform seed layers and two distinctive processes may form ZnO as the final product via the initial nucleation step consisting of the reaction between Zn^{2+} ions from respective zinc precursors and OH^- ions from H_2O.

Key words: ZnO, Nanorod, Seed layer, Atomic layer deposition, Hydrothermal growth.

Introduction

In addition to the conventional nanorods, nanowires, and nanotubes, a variety of new nanomaterials have recently emerged [1]. Because these nanomaterials have shown the remarkable properties compared to their bulk or thin film, the enormous research efforts have been made to create novel functional nanostructures to be adequate for the respective purposes and develop smart nanodevices [2]. Zinc oxide (ZnO) is one of most popular materials for nanostructure fabrication and it has a high electron mobility (>100 cm^2/Vs), wide band gap (3.37 eV), and large exciton binding energy (60 mV) with the wurtzite hexagonal structure revealing self-polarized surfaces at ambient conditions [3]. For this structural characteristics, ZnO readily forms one-dimensional (1D) tubular nanostructures and has been widely studied and used for applications in nanoelectronic devices such as gas sensor [4], light-emitting diodes [5], optical modulator waveguides [6], photodetector [7], surface acoustic wave filter [8], solar cells [9], and varistors [10]. In research on ZnO nanostructure growth, various chemical, electrochemical, and physical synthesis methods to construct highly oriented arrays of anisotropic ZnO nanorods have been widely studied and developed. For example, vapor-liquid-solid (VLS) growth [11], metal-organic chemical vapor deposition (MOCVD) [12], pulsed laser deposition (PLD) [13], templating with anodic alumina membranes [14], and epitaxial electrodeposition [15] have been successful in growing c-axis aligned ZnO nanorod arrays. However, these methods commonly require relatively high temperature (400-800 °C) and include cumbersome multiple growth processes.

In recent years, the synthesis of ZnO nanorods by hydrothermal solution method has been constantly reported [16]. This technique has shown more technical benefits compared to others such as low temperature processes (<100 °C) and large-scale fabrication at low cost. For hydrothermal solution method, the morphology of ZnO nanorod arrays can be changed by adjusting their growth conditions such as concentration and pH of precursor solution, growth temperature and time, and material and thickness of seed layer [17, 18]. In particular, thickness of seed layer plays a significant role in the density, diameter, and height of highly oriented ZnO nanorods [19]. Liu et al. reported that the aspect ratio of ZnO nanowires increased by 100 times and their density enormously increased more than 5 orders of magnitude as varying the seed layer thickness from 1.5 nm to 3.5 nm using sputtering technique [20].

In this article, we precisely controlled the thickness of ZnO seed layer using atomic layer deposition (ALD) and thereby investigated the change of the morphology of the nanorod array during the hydrothermal ZnO deposition on the seed layer. ALD is based on self-

[1]contributed equally to this work.
*Corresponding author:
Tel : +82-2-2220-0387
Fax: +82-2-2292-3523
E-mail: hjeon@hanyang.ac.kr

limited surface reactions as one of the chemical vapor deposition (CVD) method [21]. As this technique allows obtaining highly conformal and uniform thin layer due to the layer by layer construction of materials, it is a viable means with the ability to manipulate its excellent thickness and composition and to create pinhole-free films at high density [22]. This excellent controllability of ALD allows ultrathin ZnO seed layers deposited on diverse substrates to serve as the template layer for the nanorod arrays. Therefore, this study shows that ZnO seed layer grown by ALD successfully tuned the morphology of ZnO nanorod arrays.

Experimental

This study focuses on development of technical method for control of the morphology of ZnO nanorods, including the density, diameter, and height, by varying the thickness of ultrathin ZnO seed layer. First, we used 100 nm thick SiO_2 wafers as the substrate to deposit ultrathin ZnO seed layers with different thickness. These seed layers were formed by ALD using diethylzinc (DEZ, $Zn(CH_2CH_3)_2$) and deionized water (H_2O) as Zn and oxidant precursors, respectively. In ALD process, argon gas was used as a carrier and purge gas. Also, the temperature was set at 150 °C, and the operation pressure was maintained at 0.5 Torr. The thickness of ZnO seed layer was varied by increasing the reaction cycle, i.e., 6 to 16 cycles with an increment of 2 cycles. The growth rates of ZnO thin film were 0.2 nm per cycle, and its thickness ranged from 1.2 nm to 3.2 nm.

In order to grow the ZnO nanorods on the seed layer, we conducted the hydrothermal nanocrystal synthesis. In this process, an equimolar aqueous solution (0.02 M) of zinc nitrate hexahydrate [$Zn(NO_3)_2 \cdot 6H_2O$, Sigma Aldrich, 99.0% purity] and hexamethylenetetramine (HMT) [$C_6H_{12}N_4$, Sigma Aldrich, 99.0% purity] was dissolved in a Teflon beaker filled with 80 mL of deionized water. Before introducing the substrate into this solution, the Teflon beaker containing the precursor solution was maintained in a laboratory oven at 90 °C for 1 hour to reduce the density of free-floating ZnO nanoparticulates [3]. The substrate was then placed upside-down in a Teflon beaker filled with the heated solution and was held at the same temperature for 2 hours. At the end of the growth period, the sample was removed from the solution, then immediately rinsed with deionized water to extirpate any residual salt from the surface. Finally, the sample was dried naturally in laboratory air at room temperature. The morphology of ZnO nanorod arrays depends only on the thickness of ALD ZnO-coated seed layers by fixing all hydrothermal synthesis conditions used in this study.

The thickness was measured using conventional spectroscopic ellipsometer (SE, M-2000V, J.A. Woollam Co., USA) after deposition of a ZnO seed layer by ALD on planar silicon dioxide substrate, separately. The morphology and geometric parameters of ZnO nanorods were characterized using a field emission scanning electron microscope (FESEM, S-4800, HITACHI, Japan). The crystal structures were determined by high resolution transmission electron microscope (HRTEM, JEM-2010, JEOL Ltd., Japan) and X-ray diffraction (XRD, DMAX-2500, Rigaku Co., Japn). Also, the information on the chemical bonds and compositions of ZnO nanorods were analyzed using X-ray photoelectron spectroscopy (XPS, VG ESCALAB 220i-XL, Thermo Fisher Scientific Inc., USA).

Results and Discussion

In order to understand the effect of ZnO seed layer on the morphology of the nanorod arrays, the nanorods were grown on a series of samples with the seed layers at different thickness using ALD technique. The morphologies are summarized in Fig. 1. The panels on

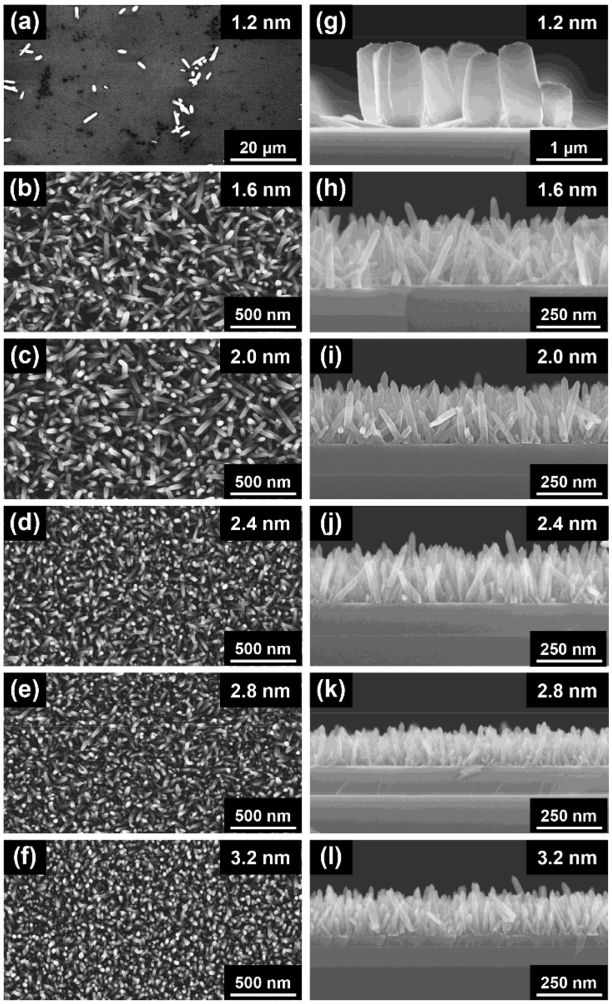

Fig. 1. (a-f) FESEM top view images of ZnO nanorods grown on a series of ZnO ALD-coated SiO_2 substrates with the areas with seed layer thickness of 1.2, 1.6, 2.0, 2.4, 2.8, and 3.2 nm, respectively. (g-l) The corresponding cross sectional view images.

Table 1. The relationship between the thickness of the ZnO seed layers controlled by the ALD cycles and geometric parameters of the nanorod.

ALD cycle	6	8	10	12	14	16
Seed thickness (nm)	1.2	1.6	2.0	2.4	2.8	3.2
Density (cm^{-2})	1.18×10^{6}	4.31×10^{10}	6.54×10^{10}	9.05×10^{10}	1.06×10^{11}	1.15×10^{11}
Mean diameter 2r (nm)	591	36	31	26	23	22
Mean height h (μm)	1.28	0.31	0.26	0.21	0.18	0.17

the left (Fig. 1(a-f)) show FESEM top view images of ZnO nanorod arrays obtained on the areas with the seed layer thickness of 1.2, 1.6, 2.0, 2.4, 2.8, and 3.2 nm, respectively. Fig. 1(g-l) are the corresponding cross sectional view images of those in Fig. 1(a-f). In these images, it is found that with the increase in the thickness of ZnO seed layer, the morphology of the nanorod arrays reveals an appreciable difference consistently. When the seed layer is thicker, the nanorod array forming on it is much denser. Surprisingly, despite the fact that ZnO seed layer thickness changed in a narrow range, i.e., from 1.2 nm to 2.8 nm, the nanorod density increased more than 5 orders of magnitude (from 1.18×10^{6} to 1.06×10^{11} cm^{-2}). On the contrary, the diameter and height of ZnO nanorods decreased as the thickness of the seed layer increases. The consequent geometric parameters are summarized in Table 1.

It is noted that there are two critical thicknesses affecting the morphology of ZnO nanorod arrays in the analysis of FESEM images as the previous work [20]. In our experiments, no nanorod forms on the seed layer with the thickness below 1.2 nm. This is the first critical thickness (1.2 nm), which is minimum one to enable ZnO nanorods to create. Only few nanorods on 1.2 nm thick seed layer are seen on the surface of the sample (Fig. 1(a) and Table 1). Also, we can observe that the increased ZnO seed layer thickness has induced comparatively slight change of the nanorod density at 2.8 nm of seed layer thickness (Fig. l(e), (f), (k), and (l)). In order to further confirm this view, the nanorods are grown on sample with a 3.2 nm thick seed layer and the density increase is not noticeable in this case (Table 1). Therefore, 2.8 nm of seed layer thickness is the second critical thickness, which shows a turnaround for increase of ZnO nanorod density.

Structural analysis on ZnO nanorods was performed using TEM. Fig. 2 shows the TEM image of a free-standing ZnO nanorod. This image shows a distance of 0.52 nm between two lattice fringes, which matches the interlayer spacing of the (002) planes in the ZnO crystal lattice. The corresponding selected area electron diffraction (SAED) pattern elucidates that ZnO nanorods is subject to the excellent single crystallinity and grows anisotropically along a preferential [0001] direction (the inset of Fig. 2). We also characterized the crystallographic properties of ZnO nanorods by XRD. Fig. 3 shows XRD spectra for vertically aligned hexagonal ZnO

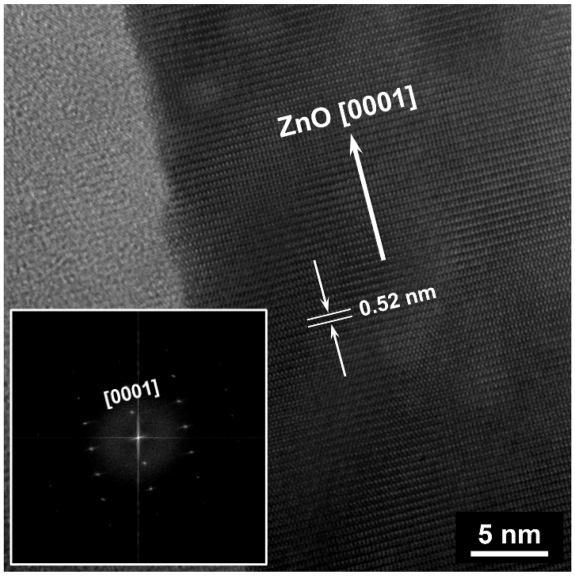

Fig. 2. HRTEM image of a free-standing ZnO nanorod. The inset is the corresponding SAED pattern.

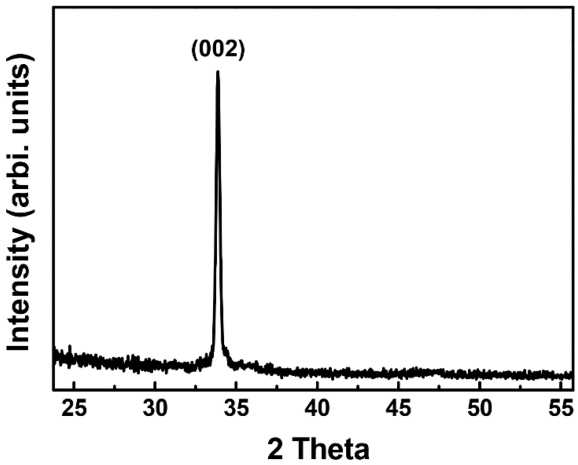

Fig. 3. XRD spectra for vertically aligned hexagonal ZnO nanorods.

nanorods. The diffraction peak of (002) plane in ZnO nanorods are observed at $2\theta = 34.28^{\circ}$ according to ZnO crystal structure [JCPDS:36-1451]. The strong intensity of (002) diffraction indicates that the nanorods are grown along the c-axis orientation. Consequently, these XRD patterns of ZnO nanorods are consistent with the TEM result as the (002) peak is related to the crystal plane of wurtzite ZnO crystal, where [0001] is the growth direction.

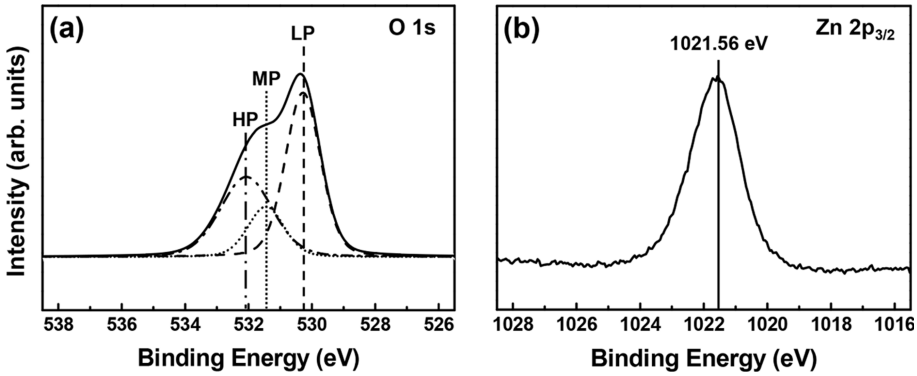

Fig. 4. XPS spectra of (a) O 1s and (b) Zn $2p_{3/2}$ spectra of sample with ZnO nanorods.

For the purpose of analyzing the surface chemical bonds and compositions in ZnO nanorods on ultrathin seed layer, XPS measurement was performed. The XPS spectrum was calibrated by taking the binding energy of the C 1s peak (285.0 eV) as a reference. Fig. 4(a) is the XPS spectra for O 1s in ZnO nanorod arrays grown on an ALD-coated seed layer. The O 1s peaks, which are centered at 530.3 eV with a shoulder at 532 eV, can be deconvoluted into three sub-peaks. The first sub-peak, with a low binding energy component (LP) of around 530.3 eV, was assigned to a Zn-O bond [23]. The second sub-peak, with a middle binding energy component (MP) of around 531.2 eV, was associated with the oxygen vacancies in oxygen-deficient regions [24], and the third sub-peak, with a high binding component (HP) of around 532.4 eV, attributed to the presence of loosely bound oxygen on the surface of the ZnO nanorods belonging to a specific species, which includes CO_3, adsorbed H_2O, or O_2 [25]. The XPS spectrum of O 1s was analyzed using a combination of Gaussian (80%) and Lorentzian (20%) fitting, and an area ratio was calculated for the three peaks corresponding to the LP, MP, and HP mentioned above. The relative intensity ratio of the low binding energy component [LP/(LP + MP + HP)] is higher than other energy components, indicating that ZnO nanorods have a major chemical bond of Zn-O. Fig. 4(b) is the XPS spectra for Zn $2p_{3/2}$ for the corresponding sample. The peak corresponding to Zn $2p_{3/2}$ is located at 1021.56 eV, which is a similar binding energy to that in the standard bulk ZnO.

In order to contemplate the effect of ZnO seed layer thickness on the morphology of the nanorod arrays, it is necessary to discuss the role of ZnO seed layer during the hydrothermal step. The seed layer thickness, which is controlled by ALD technique, is the only variable in our experiments. The hydrothermal growth of ZnO nanorod is explained by the following chemical reactions [26]:

$$(CH_2)_6N_4 + 6H_2O \rightarrow 6HCHO + 4NH_3 \quad (1)$$

$$NH_3 + H_2O \rightarrow NH_4^+ + OH^- \quad (2)$$

$$Zn^{2+} + 2OH^- \leftrightarrow Zn(OH)_2 \quad (3)$$

$$Zn(OH)_2 \leftrightarrow ZnO(s) + H_2O \quad (4)$$

In a series of reactions, the first two chemical reactions describe the formation of OH^- ions, which are supplied by reacting two reagents, i.e., zinc nitrate hexahydrate and HMT, to induce the last two. When the concentration of Zn^{2+} and OH^- ions is higher than a critical value, these ions form metastable $Zn(OH)_2$ precipitates. Because the $Zn(OH)_2$ precipitates are more soluble than the ZnO precipitates, it can continuously separate into the Zn^{2+} and OH^- ions, which form the ZnO nuclei. In the light of the chemical reaction mechanism, the crystallographic habits of wurtzite hexagonal ZnO may be considered to account for the hydrothermal ZnO nanorod growth mechanism. The ZnO structure has catalytically active polar faces and chemically inert non-polar ones [27]. As polar faces with surface dipoles are thermodynamically unstable than non-polar faces, they may undergo rearrangement to minimize their surface energy and thus have a tendency to grow more rapidly. Accordingly, the zinc and oxygen ions are arranged alternately along the [0001] direction on the polar (002) plane, which is the most rapid-growth-rate plane over other planes, and thus, ZnO nanorods are well oriented along the normal direction of the substrate surface.

It is important to note that the reaction 3 and 4 are reversible [28]. The Zn^{2+} and OH^- ions chemically react to produce the final products, that is, ZnO. Inversely, the Zn-O bonds of the seed layers can be broken, and thereby ZnO precipitates may return to primary precipitates, i.e., $Zn(OH)_2$ precipitates or the Zn^{2+} and OH^- ions as ZnO nanorods are known to be corroded away in acid conditions. In the hydrothermal solution, the growth and dissociation of ZnO competitively but simultaneously occurs in the initial nucleation steps. The reversibility, which may be mainly influenced by the diameter of the seed layer and the amounts of Zn^{2+} and OH^- ions, is largely irrelevant to the thickness of the seed layer. Notwithstanding, the seed layer thickness is the crucial factor to form the initial ZnO nuclei on the seed layer. When the seed layer thickness exceeds a critical value for the formation of ZnO nuclei, the seed layer serves as a promoter for the initial nucleation. Otherwise, neither

ZnO nuclei nor nanorods form due to the dissociation reaction. The coexistence of the growth and dissociation can underpin the view that there are the two critical thicknesses, which define the evolvement of the morphology of ZnO nanorod arrays, during the hydrothermal synthesis. The first critical thickness (i.e., with 6 ALD cycles or 1.2 nm) may be a marker for the growth and dissociation of ZnO nanorods. By increasing the thickness with more ALD cycle, its capability to sustain the dissociation will be improved gradually, and more sites on a thicker seed layer can form ZnO nuclei. ZnO nanorod arrays grown on the nuclei have much denser morphology. However, for the seed layer thicker than the second critical thickness (i.e., 14 ALD cycles or 2.8 nm), the entire surface of the seed layer may be chock-a-block with the nucleation sites. In this case, ZnO nanorod density increases slightly because of no space to create new sites (Fig. 1 and Table 1).

In the growth technique of ZnO nanorods, the introduction of the seed layer curtails interfacial lattice mismatch and thus promotes the initial nucleation, which further allows the easy morphological control of nanorod arrays. Upon varying the thickness of ZnO seed layer, which is the only variable in our experiments, by ALD, it is found that the nanorod is formed on the thinner film and the tuning scale is wider than the previous works [20,29]. This may result from ALD to the control of the seed layer thickness. ALD technique facilitates the control of the film thickness at the atomic scale by the self-limiting growth mechanism and produces densely packed, virtually defect-free, and high uniform films [21,30], which can be used to deposit high-quality ultrathin seed layer. Owing to such benefits of ALD technique, atomic layer deposited seed layer may moderate the dissociation reaction during the hydrothermal growth and make the nanorod density increase rapidly. Furthermore, although our experiments constitute two distinct processes; deposition of the seed layer using ALD followed by the hydrothermal growth, this two-step process forms ZnO as the final product via the nucleation reaction between Zn^{2+} ions from respective zinc precursors and OH^- ions from H_2O. A further study is in progress to clarify the correlation between ALD and hydrothermal growth to achieve the control technique on the morphology of ZnO nanorod arrays. Consequently, by applying ALD technique for the precise control on the seed layer thickness in nm range, the ultrathin ZnO seed layer was produced for the successful growth of the ZnO nanorods, and with a narrow change in the seed layer thickness (1.2 to 2.8 nm), the nanorod density can be changed in a wide range (1.18×10^6 to 1.06×10^{11} cm^{-2}).

Conclusions

We investigated the effect of the seed layer thickness on the density of the nanorod arrays by using ALD technique. The morphology of ZnO nanorod arrays, including the density, diameter, and height, shows a wide variation with the small increase in the seed layer thickness from 1.2 to 2.8 nm. For a very thin seed layer thinner than 1.2 nm, which is declared as the first critical thickness, no nanorod forms on ZnO thin film. The noticeable increase in ZnO nanorod density is noted between 1.2 and 2.8 nm of the seed layer but on the seed layer thicker than 2.8 nm, the change of the nanorod density is inactive. We regard that this consequence results from the coexistence of the growth and dissociation during the hydrothermal growth, which is affected by ZnO seed layer, serving as a crucial factor to control the density of the nanorods. In this study, the ALD-grown seed layer facilitates the formation and control of ZnO nanorod arrays. In addition, through the various analysis using TEM, XRD, and XPS, it is confirmed that single crystalline ZnO nanorods with strong Zn-O bonds grow anisotropically along a preferential [0001] direction. The demonstrated technique in this study on the morphology control of various ZnO nanostructures by ALD can be utilized for a wide range of future applications, such as energy conversion and storage, sensing and advanced nanodevices.

Acknowledgements

This study was supported by the National Research Foundation of Korea (NRF) grant funded by the Korean Government (MEST) (NRF-2014M3A7B4049367).

References

1. Z.R. Dai, Z.W. Pan, and Z.L. Wang, Adv. Funct. Mater. 13[1] (2003) 9-24.
2. L. Vayssieres and M. Graetzel, Angew. Chem. Int. Edit. 43[28] (2004) 3666-3670.
3. J.-S. Na, B. Gong, G. Scarel, and G.N. Parsons, Acs Nano 3[10] (2009) 3191-3199.
4. N. Golego, S.A. Studenikin, and M. Cocivera, J. Electrochem. Soc. 147[4] (2000) 1592-1594.
5. M.-C. Jeong, B.-Y. Oh, M.-H. Ham, S.-W. Lee, and J.-M. Myoung, Small 3[4] (2007) 568-572.
6. J.Y. Lee, Y.S, Choi, J.H. Kim, M.O. Park, and S. Im, Thin Solid Films 403 (2002) 553-557.
7. S. Liang, H. Sheng, Y. Liu, Z. Huo, Y. Lu, and H. Shen, J. Cryst. Growth. 225 (2001) 110-113.
8. N.W. Emanetoglu, C. Gorla, Y. Liu, S. Liang, and Y. Lu, Ma.t Sci. Semicon. Proc. 2[3] (1999) 247-252.
9. M. Law, L.E. Greene, J.C. Johnson, R. Saykally, and P. Yang, Nat. Mater. 4 (2005) 455-459.
10. Y. Lin, Z. Zhang, Z. Tang, F. Yuan, and J. Li, Adv. Mater. Opt. Electr. 9[5] (1999) 205-209.
11. H.T. Ng, J. Han, T. Yamada, P. Nguyen, Y.P. Chen, and M. Meyyappan, Nano Lett. 4[7] (2004) 1247-1252.
12. E. Galoppini, J. Rochford, H. Chen, G. Saraf, Y. Lu, A. Hagfeldt, and G. Boschloo, J. Phys. Chem. B 110[33]

(2006) 16159-16161.
13. J.H. Choi, H. Tabata, and T. Kawai, J. Cryst. Growth 226[4] (2001) 493-500.
14. Y. Li, G.W. Meng, L.D. Zhang, and F. Phillipp, Appl. Phys. Lett. 76[15] (2000) 2011-2013.
15. R. Liu, A.A. Vertegel, E.W. Bohannan, T.A. Sorenson, and J.A. Switzer, Chem. Mater. 13[2] (2001) 508-512.
16. L. Vayssieres, Adv. Mater. 15[5] (2003) 464-466.
17. B. Cao and W. Cai, J. Phys. Chem. C 112[3] (2008) 680-685.
18. Z.R. Tian, J.A. Voigt, J. Liu, B. McKenzie, M.J. McDermott, M.A. Rodriguez, H. Konishi, and H. Xu, Nat. Mater. 2 (2003) 821-826.
19. T. Ma, M. Guo, M. Zhang, Y. Zhang, and X. Wang, Nanotechnology 18[3] (2007) 035605.
20. J. Liu, J. She, S. Deng, J. Chen, and N. Xu, J. Phys. Chem. C 112[31] (2008) 11685-11690.
21. M. Leskela and M. Ritala, Angew. Chem. Int. Edit. 42[45] (2003) 5548-5554.
22. S.M. George, Chem. Rev. 110[1] (2010) 111-131.
23. B.J. Coppa, R.F. Davis, and R.J. Nemanich, Appl. Phys. Lett. 82[3] (2003) 400-402.
24. Z.G. Wang, X.T. Zu, S. Zhu, and L.M. Wang, Physica E 35[1] (2006) 199-202.
25. S. Lee, S. Bang, J. Park, S. Park, W. Jeong, and H. Jeon, Phys. Status Solidi A 207[8] (2010) 1845-1849.
26. Q. Ahsanulhaq, A. Umar, and Y.B. Hahn, Nanotechnology 18[11] (2007) 115603.
27. P.X. Gao and Z.L. Wang, J. Phys. Chem. B 108[23] (2004) 7534-7537.
28. A. Wei, X.W. Sun, C.X. Xu, Z.L. Dong, Y. Yang, S.T. Tan, and W. Huang, Nanotechnology 17[6] (2006) 1740.
29. J. Song and S. Lim, J. Phys. Chem. C 111[2] (2007) 596-600.
30. J.L. van Hemmen, S.B.S. Heil, J.H. Klootwijk, F. Roozeboom, C.J. Hodson, M.C.M. van de Sanden, and W.M.M. Kessels, J. Electrochem. Soc. 154[7] (2007) G165-169.